A Model Reference Friction Observer for Friction Compensation and Shaping in Interaction Control

Abstract— **Friction phenomena may significantly deteriorate the performance and reliability of force-controlled systems. Despite existing solutions, achieving accurate and robustly stable friction compensation is challenging due to model inaccuracies and parameter identification issues. This paper proposes a force control architecture with accurate friction compensation and friction shaping capabilities, based on a novel model reference approach. Since passivity is a fundamental requirement for interaction control, this work investigates under which conditions the proposed approach preserves passivity at the environment, control, and friction ports. This implies that the proposed architecture can passively compensate for any type of friction and can be combined with any passive force controller while guaranteeing a stable interaction with any passive environment. The approach is validated using simulation and experimental trials.**

I. INTRODUCTION

Nowadays, interaction control is a well-established technology with applications spanning various domains, including industry [1], medical applications [2] and assistive technologies [3]. In practical scenarios, however, force-controlled systems are affected by mechanical friction, which can significantly compromise their performance and reliability.

Friction compensation is an established research topic and many solutions have been proposed over the years. Model-based friction compensation is a widely used approach [4]–[6], typically implemented as a feedforward control action with friction parameters identified offline. Common friction models include the exponential model [7], the Dahl model [8], and the LuGre model [9]. However, the effectiveness of model-based compensation is often limited, as friction parameters are highly sensitive to factors like temperature and wear. Moreover, accurately identifying dynamic friction parameters can be time-consuming. For example, as noted in [10], estimating bristle stiffness and damping requires dedicated experiments under nominal conditions. As a consequence, the estimation of such dynamic parameters is often neglected [11]–[13]. To account for time-varying parameters, adaptive strategies have been proposed [14], [15], including the use of machine learning technologies such as neural networks [16], [17]. Unfortunately, such approaches are only suitable for position (or velocity) control and not in the case of force control, since they rely on information from position error.

Friction Observers (FOBs) offer a promising model-free[1] alternative for friction estimation and compensation. However, existing FOBs have been developed exclusively for position- or velocity-controlled systems [18]–[20]. To the best of the authors' knowledge, model-free FOBs have not yet been applied to interaction control scenarios. As a result, their applicability, stability characteristics, and potential benefits in this context still need to be investigated. For instance, not all friction is undesirable in interaction control applications. Viscous friction can be particularly beneficial as it improves interaction control performance and stability [21], [22]. Conversely, Coulomb friction, stiction, and stick-slip phenomena are undesirable, as they are associated with static errors and limit cycle vibrations [23].

Alternatively to FOBs, if we consider existing Disturbance Observers (DOBs) designed for force control applications, the DOB action rejects both disturbances due to friction and to the interacting environment without clearly distinguishing them [24], [25]. Unfortunately, this may lead DOBs to significantly deteriorate stability, as shown in [26]. Alternative solutions to conventional DOBs consider the so-called reaction torque/force observer (RTOB/RFOB). These approaches can distinguish between friction forces and environmental forces but just for interaction torque estimation purposes and not for friction compensation [27], [28].

In summary, current friction compensation methods for force control exhibit the following limitations:

1) Model-based approaches offer stable compensation—since feedforward actions do not compromise system stability—but often lack accuracy due to model complexity and parameter uncertainties. Despite these drawbacks, they remain widely used;
2) Existing DOB architectures do not distinguish between disturbances due to friction and to the interacting environment. As a consequence, they may pose severe stability issues depending on the environment dynamics [26];

In light of these considerations, this paper introduces a novel force control architecture that includes a Model Reference Friction Observer (MR-FOB). This observer allows to (1) accurately compensate undesired friction effects without relying on a friction model and (2) shape the desired viscous friction profile accordingly to the reference model, to enhance force control performance. The latter property is of paramount importance in interaction control and has never been addressed in previous works on FOBs and DOBs.

Since passivity is a fundamental requirement in force control, a passivity analysis is proposed to outline under which conditions the proposed architecture can guarantee coupled stability with an unknown passive environment. Results show

[1]In this paper, the term "model-free" is used specifically in reference to the friction model and not to the system model. This means that the observer does not rely on a predefined friction model.

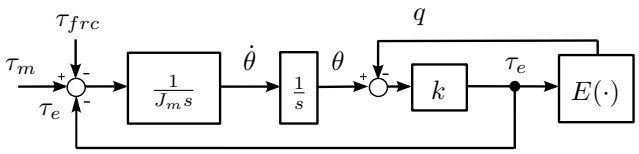

Fig. 1: Block diagram of the considered system modelling.

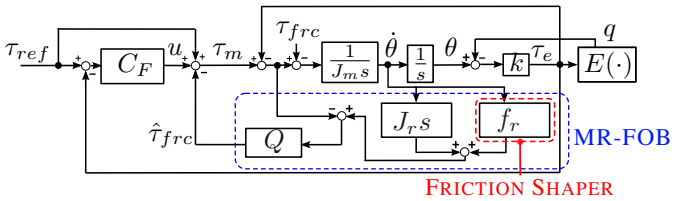

Fig. 2: Block diagram of the proposed MR-FOB architecture.

that the MR-FOB preserves passivity of the force-controlled system by satisfying a simple condition on the observer parameters. As a consequence, the MR-FOB can be used in combination with any passive force controller, leading to a stable interaction with any passive environment. Moreover, the friction compensation action of the MR-FOB preserves passivity for any friction profile, including nonlinear friction dynamics such as stiction.

Although the analysis focuses on 1-degree-of-freedom (DoF) systems, the proposed architecture can be easily extended to multi-DoF manipulators by implementing the MR-FOB schema at each joint. The only requirement is to have joint torque measurements available at each joint.

The paper is organized as follows. Section II briefly describes the considered system model and introduces our notation. Section III presents the proposed architecture and theoretically motivates its passivity properties. The proposed approach is then validated in simulations (in Section IV) and experimentally (in Section V) considering different interacting environments and diverse friction phenomena affecting the actuator dynamics. Conclusions are drawn in Section VI.

II. SYSTEM MODELLING

This Section describes the considered system model and introduces our notation. A block diagram representation of an actuator interacting with a generic environment $E(\cdot)$ is shown in Figure 1. Such a diagram describes an actuator having reflected inertia J_m, a generic friction torque profile given by τ_{frc} (which includes the linear profile $\dot{\theta} f_m$ with f_m as viscous friction coefficient) and a series stiffness k. The series stiffness models a force sensor or a purposely added series elastic element [29], [30]. The generic environment $E(\cdot)$ may eventually include the robot link dynamics. The system can be modeled using the following equations:

$$\begin{aligned} J_m \ddot{\theta} &= \tau_m - \tau_e - \tau_{frc} \\ \tau_e &= k(\theta - q) \end{aligned} \tag{1}$$

where θ is the motor angle, q is the joint angle and τ_m is the motor torque at the output shaft (which is proportional to the current and accounts for an eventual gear reduction). The torque τ_e is due to the environment interaction and can be measured considering the deformation of a torque sensor, a series spring [29] or a flexible link [30].

III. A MODEL REFERENCE FRICTION OBSERVER

The proposed architecture is shown in Figure 2. In this schema, Q is a first-order low-pass filter with cutoff frequency ω_q, which is used to both allow the model inversion and to tune the frequency up to which friction-related disturbances are rejected. $J_r > 0$ is the reference actuator inertia while $f_r \geq 0$ represents the reference viscous friction coefficient which can be eventually adjusted to shape the friction profile. Differently from existing approaches, we assume that the observer parameters J_r and f_r may significantly differ from the real plant, and the designer can tune these parameters to satisfy the passivity condition (as detailed in Section III-B) and for friction-shaping (as detailed in Section III-C).

Coming back to the block diagram, C_F is a generic force controller and the desired torque τ_{ref} is used as a feed-forward term. In our notation, the MR-FOB is implemented as:

$$\tau_m = u - [(J_r s + f_r)\dot{\theta} - (\tau_m - \tau_e)]Q(s) \tag{2}$$

where u is the feedback part of the force control law.

A. Comparison with Traditional DOBs and RTOBs

This subsection highlights how the proposed architecture differs from traditional DOBs [24], [31] or RTOBs [27], [28]. Regarding traditional DOBs, the proposed MR-FOB architecture is different for the following reasons:

1) *Friction Rejection:* the MR-FOB input is not only τ_m, instead it is the difference between τ_m and τ_e. The interaction torque τ_e brings information on the environment dynamics in order to reject exclusively friction-related disturbances while ignoring environment-related disturbances. Instead, conventional DOBs are designed to reject not only friction but also environment-related disturbances.

2) *Model Reference:* none of the existing DOBs relies on a goal-driven reference model. Instead, they assume a nominal model with fixed parameters that must closely match the real system model to ensure stability [32].

Regarding RTOBs, they are designed for a fundamentally different purpose: estimation of the interaction torque. RTOBs cannot provide any estimation of friction forces; instead, in these applications, it is "important to know the friction forces a priori and as accurately as possible" to ensure high estimation performance [27].

The only similar architecture we could find is the FOB introduced in [18]. However, this observer has been designed for position-controlled architecture, without any passivity guarantee and without any friction-shaping capability.

B. Passivity Analysis

It is established that negative feedback connection of passive systems is still passive, thus stable. It can be observed in Figure 3a and 3b that both the environment and the controller are connected in negative feedback to the system

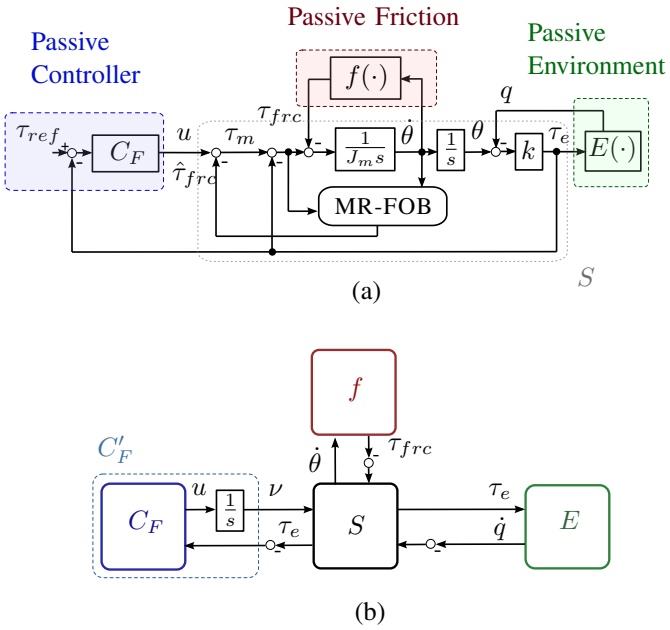

Fig. 3: Block diagram of the proposed architecture highlighting the interconnection of passive blocks (a), arranged to put in evidence the control port $(-\tau_e, \nu)$, the environment port $(-\tau_e, \dot{q})$ and the friction port $(\dot{\theta}, -\tau_{frc})$ (b).

S, which includes the actuator and the MR-FOB. By taking advantage of these negative feedback interconnections, the following lemma proves (I) passivity of the MR-FOB at the environment port $(-\tau_e, \dot{q})$ and (II) passivity of the MR-FOB at the control port $(-\tau_e, \nu)$ with $\dot{\nu} = u$. The former guarantees a stable interaction with any passive environment while the latter implies that the MR-FOB can be used in combination with any force controller that is passive at the port $(-\tau_e, \nu)$, while retaining a stable interaction with any passive environment. For instance, a PD controller ensures passivity at the port (-τ_e,ν) whereas a PID controller does not.

In the following proof τ_{frc} is set to 0 which allows to guarantee that the MR-FOB architecture is passive even in case of no mechanical dissipation. This represents a worst-case condition for passivity. Moreover, we disregard for the moment any friction shaping capability and we set $f_r = 0$.

Lemma 1: The system described by (1) with $\tau_{frc} = 0$ under the feedback action of the proposed MR-FOB law (2) preserves passivity at the environment port $(-\tau_e, \dot{q})$ and at the control port $(-\tau_e, \nu)$ iff

$$J_r \geq J_m \tag{3}$$

Proof: The system (1) with the MR-FOB (2) can be arranged as:

$$-\tau_e = Z_{\dot{q}}(s)\dot{q} + Z_{\nu}(s)\nu \tag{4}$$

where $Z_{\dot{q}}(s)$ is the impedance seen at the environment port $(-\tau_e, \dot{q})$ and $Z_{\nu}(s)$ is the impedance seen at the control port $(-\tau_e, \nu)$.[2]

$Z_{\dot{q}}(s)$ can be computed as:

$$Z_{\dot{q}}(s) = \frac{k(J_m s^2 + J_r \omega_q s)}{J_m s^3 + J_r \omega_q s^2 + ks + k\omega_q}. \tag{5}$$

Stability of (5) can be proved using the Root-Hurwitz criterion, which leads to the following stability condition:

$$J_r \geq J_m \tag{6}$$

By computing $\mathrm{Re}[Z_{\dot{q}}(j\omega)]$, one finds:

$$\mathrm{Re}[Z_{\dot{q}}(j\omega)] = \frac{-kJ_m\omega^2\alpha + kJ_r\omega_q\omega\beta}{\alpha^2 + \beta^2} \tag{7}$$

where $\alpha = k\omega_q - J_r\omega_q\omega^2$ and $\beta = k\omega - J_m\omega^3$. Solving for $Re[Z(j\omega)] \geq 0$ the following condition is derived:

$$J_r \geq J_m \tag{8}$$

Thus, the combination of conditions (6) and (8) results in the passivity condition as expressed in (3).

The impedance $Z_{\nu}(s)$ seen at the control port can be computed as:

$$Z_{\nu}(s) = \frac{ks(s + \omega_q)}{J_m s^3 + J_r \omega_q s^2 + ks + k\omega_q} \tag{9}$$

Similarly to the case of $Z_{\dot{q}}(s)$, it can be verified that $Z_{\nu}(s)$ is stable under condition (6) since it has the same denominator of (5). $\mathrm{Re}[Z_{\nu}(j\omega)]$ can be computed as:

$$\mathrm{Re}[Z_{\nu}(j\omega)] = \frac{-k\omega^2\alpha + k\omega\omega_q\beta}{\alpha^2 + \beta^2}, \tag{10}$$

and it can be verified that $\mathrm{Re}[Z_{\nu}(j\omega)] \geq 0$ is satisfied under condition (8). This leads to the passivity condition (3). ■

In conclusion, the passivity condition (3) reveals that if the parameter J_r is equal to or *overestimates* the real motor inertia J_m, a passive interaction is always guaranteed for any passive force controller. Given the importance of the passive interaction paradigm, this represents a main novelty with respect to existing FOB/DOB approaches. Finally, given that friction observers may generate energy during stiction compensation [19], the following analysis demonstrates that the MR-FOB preserves passivity for any nonlinear friction profile, including stiction, Coulomb friction and Stribeck effects.

Passivity is proved by taking advantage of the negative feedback interconnection of the nonlinear passive map $f(\cdot)$ represented in red in Figure 3a and highlighted in Figure 3b. Since any friction dynamics, being linear or nonlinear, is inherently passive, one can consider the admittance seen at the friction port $(\dot{\theta}, -\tau_{frc})$ and prove passivity of the MR-FOB at such port. This overcomes the assumption $\tau_{frc} = 0$ of Lemma 1.

[2]Given $y = Z(s)u$, the system is passive at the port (u, y) iff (1) $Z(s)$ has no poles in the right-half plane and (2) $Re[Z(j\omega)] \geq 0\, \forall \omega \in \Re$ [33].

Lemma 2: The system described by (1) under the feedback action of the proposed MR-FOB law (2) preserves passivity at the friction port $(\dot{\theta}, -\tau_{frc})$ iff

$$J_r \geq J_m \tag{11}$$

Proof: The admittance $Z_{\dot{\theta}}(s)$ seen at the friction port is:

$$Z_{\dot{\theta}}(s) = \frac{s + 2\omega_q}{s(J_m s + (J_m\omega_q + J_r\omega_q))} \tag{12}$$

which is a stable transfer function. One can compute $\mathrm{Re}[Z_{\dot{\theta}}(j\omega)]$ as:

$$\mathrm{Re}[Z_{\dot{\theta}}(j\omega)] = \frac{\omega_q(J_r - J_m)}{\omega^2 J_m^2 + \omega_q^2(J_m + J_r)^2}. \tag{13}$$

It is straightforward to observe that, solving for $\mathrm{Re}[Z_{\dot{\theta}}(j\omega)] \geq 0$, leads to condition (11). ■

Since conditions (3) and (11) are the same, a main result of this section is that by simply satisfying $J_r \geq J_m$, one can guarantee passivity at the environment, control, and friction ports.

C. Friction-Shaping Capability

Thanks to its friction-shaping capability, the proposed MR-FOB allows designers to actively shape the viscous friction component f_r while rejecting nonlinear or undesirable friction effects. In particular, when $f_r = 0$, the MR-FOB performs full friction compensation; when $f_r > 0$, the MR-FOB can compensate or inject friction depending on actual and reference friction profiles.

The following lemma proves that, if $J_r \geq J_m$, the MR-FOB architecture preserves passivity at the environment, control, and friction ports $\forall f_r > 0$. This guarantees passivity for any linear friction shaping, thereby extending the results of Lemmas 1 and 2, which assumed $f_r = 0$.

Lemma 3: The system described by (1) under the feedback action of the MR-FOB law (2) with $J_r \geq J_m$ preserves passivity at the environment port $(-\tau_e, \dot{q})$, at the control port $(-\tau_e, \nu)$ and at the friction port $(\dot{\theta}, -\tau_{frc})$ $\forall f_r > 0$.

Proof: Passivity at the environment and at the control ports can be proved by including f_r in (5) and in (9) which results in the following impedance relations:

$$Z_{\dot{q}}(s) = \frac{J_m k s^2 + J_r k\omega_q s + f_r k\omega_q}{J_m s^3 + J_r\omega_q s^2 + (k + f_r\omega_q)s + k\omega_q} \tag{14}$$

and

$$Z_{\nu}(s) = \frac{ks(s + \omega_q)}{J_m s^3 + J_r\omega_q s^2 + (k + f_r\omega_q)s + k\omega_q}. \tag{15}$$

It can be proved that $Z_{\dot{q}}(s)$ and $Z_{\nu}(s)$ are stable $\forall f_r > 0$. Also, it can be easily verified that $\mathrm{Re}[Z_{\dot{q}}(j\omega)] \geq 0$ and $\mathrm{Re}[Z_{\nu}(j\omega)] \geq 0$ hold $\forall f_r > 0$.

Passivity at the friction port can be proved by including f_r in (12) which leads to:

$$Z_{\dot{\theta}}(s) = \frac{s + 2\omega_q}{J_m s^2 + (J_m + J_r)\omega_q s + f_r} \tag{16}$$

Parameter	Symbol	Simulation	Validation
FRICTION PARAMETERS			
Bristle stiffness	σ_0	260 N m	–
Bristle damping	σ_1	0.6 N m s/rad	–
Viscous friction	f_m	0.01 N m s/rad	0.26 N m s/rad
Stiction	f_s	0.5 N m	0.439 N m
Coulomb friction	f_c	0.4 N m	0.401 N m
Stribeck velocity	v_s	0.1 rad/s	0.01 rad/s
SYSTEM PARAMETERS			
Actuator inertia	J_m	0.14 kg m^2	0.14 kg m^2
Spring stiffness	k	58 N m/rad	58 N m/rad
CONTROL PARAMETERS			
Proportional Gain	P	5	5
Derivative Gain	D	0.1	0.1
MR-FOB Cutoff Freq.	ω_q	100 Hz	20 Hz

TABLE I: Parameters (set or estimated) used in simulation and experimental trials.

and again it can be verified that $Z_{\dot{\theta}}(s)$ is stable and $\mathrm{Re}[Z_{\dot{\theta}}(j\omega)] \geq 0$ is satisfied $\forall f_r > 0$. ■

D. Discussion of Theoretical Results

By combining Lemmas 1, 2 and 3, the overall results of this work can be summarized as follows: when the proposed architecture (Figure 2) is used and the condition $J_r \geq J_m$ is satisfied, passivity is ensured at the environment, friction, and control ports, without limitation on linear friction shaping. From a theoretical point of view, the condition $J_r \geq J_m$ is a necessary and sufficient condition. However, by incorporating τ_{frc} in Lemma 1, $J_r \geq J_m$ becomes just a sufficient condition. For the sake of completeness, a necessary and sufficient condition for passivity at the environment and control ports is reported in the following lemma, assuming a simple viscous friction model, i.e., $\tau_{frc} = f_m\dot{\theta}$.

Lemma 4: The system described by (1) with $\tau_{frc} = f_m\dot{\theta}$ under the feedback action of the proposed MR-FOB law (2) preserves passivity at the environment port $(-\tau_e, \dot{q})$ and at the control port $(-\tau_e, \nu)$ iff

$$f_m \geq (J_m - J_r)\omega_q \tag{17}$$

Proof: By including $\tau_{frc} = f_m\dot{\theta}$ in (5) and (9) it can be proved that $Z_{\dot{q}}(s)$ and $Z_{\nu}(s)$ are stable if (17) is satisfied. Also, it can be verified that $\mathrm{Re}[Z_{\dot{q}}(j\omega)] \geq 0$ and $\mathrm{Re}[Z_{\nu}(j\omega)] \geq 0$ under the same condition. ■

This result indicates that it is possible to underestimate J_m while preserving passivity at the environment and control ports. However, this requires accurate knowledge of the real friction dynamics (which is the unknown quantity). In conclusion, it is recommended to overestimate J_m to always ensure passivity preservation.

IV. SIMULATION RESULTS

The objectives of this section are: (a) to validate the passivity findings of Section III, and (b) to show the MR-FOB accuracy by using simulation tools where friction forces are

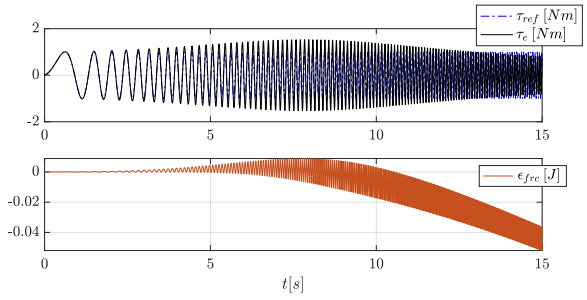

(a) $J_r = 0.9J_m$

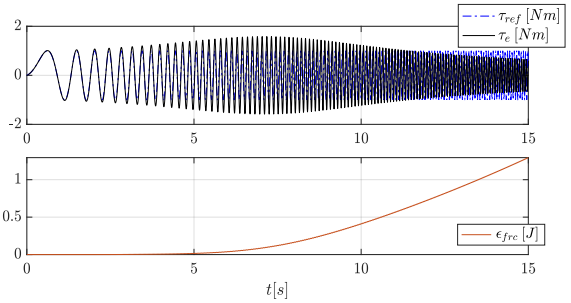

(b) $J_r = 1.1J_m$

Fig. 4: Simulations showing the energy balance of the system under the friction compensation action of the MR-FOB. In Figure (a), the reference inertia J_r is underestimated (passivity violation) while in Figure (b) it is overestimated (passivity preservation).

known.

Simulations are carried out in MATLAB/Simulink and use Runge-Kutta discretization with a fixed integration step of 10^{-4} s. The system shown in Figure 1 is modeled using the parameters reported in Table I. The friction torque τ_{frc} is modeled according to the well-known LuGre friction model [9]:

$$\begin{aligned} \tau_{frc} &= \sigma_0 z + \sigma_1 \dot{z} + f_m \dot{\theta} \\ \dot{z} &= \dot{\theta} - \sigma_0 \frac{|\dot{\theta}|}{g(\dot{\theta})} z \end{aligned} \tag{18}$$

where $g(\dot{\theta}) = f_c + (f_s - f_c)e^{-(\dot{\theta}/v_s)^2}$. The parameters of the dynamic friction model are taken from [10] while Coulomb (f_c), stiction (f_s), and Stribeck (v_s) parameters are augmented to emphasize their undesirable effect. The considered force controller is a simple PD tuned to provide a control bandwidth around 15 Hz when interacting with a high-impedance environment. This leads to P = 5 and D = 0.1. The interacting environment is assumed to be passive and is modeled as a linearized second-order system defined as $E(s) = J_e s^2 + d_e s + k_e$, where J_e is the inertia, d_e is the damping, and k_e is the stiffness. Finally, the cutoff frequency ω_q of the MR-FOB is set to 100 Hz.

A detailed description of each simulation is given in the following subsections.

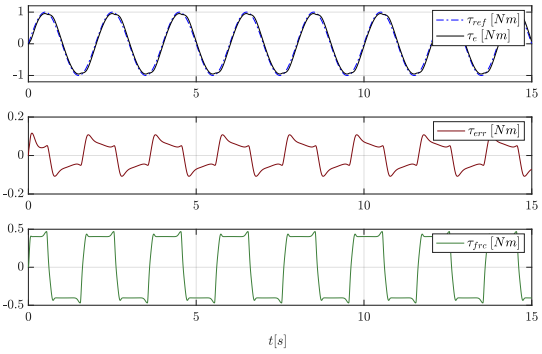

(a) PD

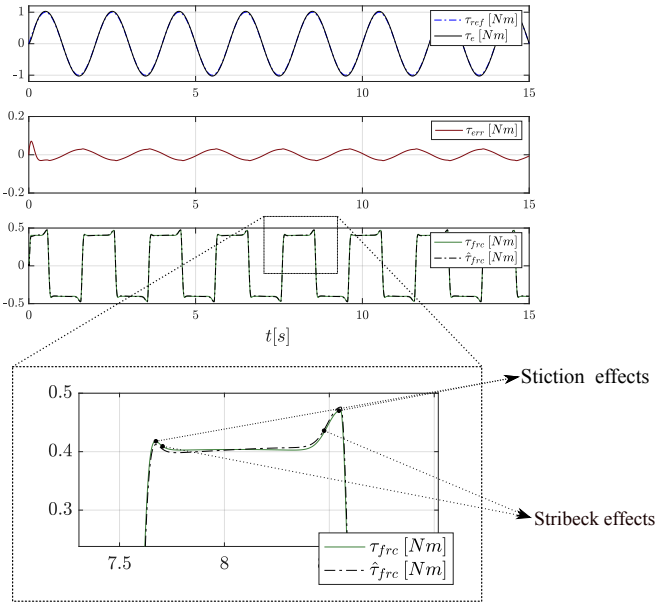

(b) PD + MR-FOB

Fig. 5: Torque tracking simulation to assess the MR-FOB friction compensation accuracy.

A. Assessing MR-FOB Passivity

The first simulations are designed to verify whether passivity is preserved by satisfying the passivity condition of Section III. Let us define the energy dissipated by the plant as:

$$E_{frc}(t) = \int_0^t \dot{\theta}(t)\tau_{frc}(t)dt \tag{19}$$

Similarly, the energy generated by the MR-FOB is defined as:

$$E_{MR-FOB}(t) = \int_0^t \dot{\theta}(t)\hat{\tau}_{frc}(t)dt \tag{20}$$

Let us define $\epsilon_{frc}(t) = E_{frc}(t) - E_{MR-FOB}(t)$. Passivity is preserved if $\epsilon_{frc}(t) \geq 0 \quad \forall t \geq 0$.

Simulation results are shown in Figure 4. In each plot, τ_{ref} represents the torque reference which is set as sweep signal reaching 15 Hz after 15 s while τ_e represents the interaction torque. The interacting environment is modeled as a high-impedance system having J_e = 1 kg m^2 and k_e =

$1{,}000\,\mathrm{N\,m/rad}$. Looking at Figure 4a, it can be observed that inertia overestimation always ensures energy dissipation ($\epsilon_{frc}(t) \geq 0$), confirming the theoretical results in Section III. Otherwise, when the passivity condition is violated, the energy generated by the MR-FOB may become higher than the energy dissipated by friction ($\epsilon_{frc}(t) < 0$).

B. Assessing MR-FOB Accuracy

The objective of this subsection is to evaluate the MR-FOB accuracy during torque tracking under the action of a simulated friction torque τ_{frc} given by (18). Since the effects of stiction, Stribeck, and Coulomb friction are dominant at low speeds [10], a low-frequency sinusoidal profile is considered as torque reference τ_{ref}. In these simulations, the torque-controlled robot interacts with a critically damped soft environment having inertia J_e = $0.01\,\mathrm{kg\,m^2}$ and stiffness k_e = $10\,\mathrm{N\,m/rad}$ to test a worst-case condition.
Results are reported in Figure 5 where $\tau_{err} = \tau_{ref} - \tau_e$. Figure 5a considers a PD force control without any friction compensation law while Figure 5b considers the same PD controller combined with the MR-FOB. Within the MR-FOB architecture, the term J_r is set 10% higher than the real J_m to preserve the passivity properties of the system, while f_r is set equal to 0 (friction is fully compensated).
By looking at Figure 5a it can be observed that a pure PD controller is unable to dominate the effects of friction, which significantly affects the error dynamics τ_{err} (RMSE = $0.071\,\mathrm{N\,m}$). Differently, Figure 5b shows accurate torque tracking thanks to the friction compensation action of the MR-FOB, even without any knowledge of friction parameters (RMSE = $0.02\,\mathrm{N\,m}$). The accuracy of friction estimation can be qualitatively observed in the third plot of Figure 5b, where $\hat{\tau}_{frc}$ denotes the estimated friction torque. It can be seen that the MR-FOB is able to accurately observe the friction profile including stiction and Stribeck effects, which are usually hard to be captured in model-free approaches [19].

V. EXPERIMENTAL RESULTS

Friction compensation capabilities of the proposed architecture are experimentally compared with a widely used model-based strategy, considering a single DoF force-controlled system interacting with two different environments: a low impedance environment and a high impedance environment. The considered friction model includes stiction, Coulomb and viscous friction, together with the Stribeck effect. Dynamic friction parameters are not considered in this validation due to the complexity involved in their identification. The considered friction model can be expressed as

$$\tau_{frc} = [f_c + (f_s - f_c)e^{-(\dot{\theta}/v_s)^2}]\mathrm{sgn}(\dot{\theta}) + f_m\dot{\theta}. \qquad (21)$$

The parameters were identified following a procedure similar to that shown in [10] while estimated parameters are reported in Table I. The following subsections describe the experimental setup and the results.

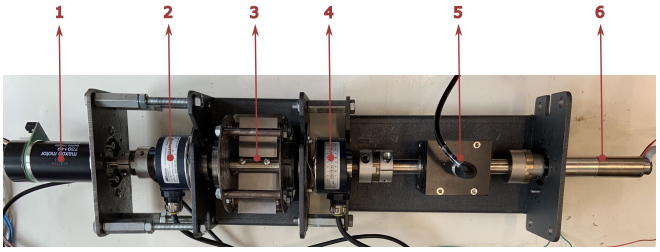

Fig. 6: A picture of the experimental setup.

A. Experimental Setup

A picture of the experiment testbed is shown in Figure 6. The testbed is composed by an actuator (Maxon EC45 flat with a 91:1 gearbox) with inertia J_m = $0.14\,\mathrm{kg\,m^2}$ (1) connected in series to a torsional spring with stiffness k = $58\,\mathrm{N\,m/rad}$ (3), followed by a torque sensor (not used in this work) (5) which is finally linked to a Virtual Environment Actuator (VEA) (6). The VEA is able to display a wide range of different interacting environments by exploiting impedance and admittance-based controllers, see [34] for details. Such environments are described in terms of desired inertia J_e, stiffness k_e, and damping d_e. Two optical encoders (2) and (4) are used to measure, respectively, the motor position θ and the environment position q. The feedback torque τ_e is measured using spring displacement. Motors are driven in current control mode using a commercial driver (ESCON 50/5) while the force control algorithms run on an embedded board (Nucleo F446RE) as periodic $2{,}000\,\mathrm{Hz}$ real-time processes.

B. Experiments Description and Results

The same PD force controller used in the simulation is considered for the experiments (P = 5 and D = 0.1). The MR-FOB cutoff frequency ω_q is set to $20\,\mathrm{Hz}$ to attenuate high-frequency sensor noise while the term J_r is again set 10% higher than the real J_m to preserve passivity. The considered torque reference is a $0.2\,\mathrm{Hz}$ square wave profile defined as $\tau_{ref}(t) = 0.6 + 0.2\mathrm{sgn}(\sin(2\pi 0.2t)$. A description of the experiments is given in the following. During the first 15 seconds, the VEA is controlled to display a critically damped soft environment expressed as J_e = $0.001\,\mathrm{kg\,m^2}$ and k_e = $5\,\mathrm{N\,m/rad}$. Then, in the last part of the experiment, the VEA is controlled to render a high-impedance environment having J_e = $1\,\mathrm{kg\,m^2}$ and k_e = $100\,\mathrm{N\,m/rad}$. The experiment is repeated considering the PD without any friction compensation law, the PD combined with the model-based approach, the PD combined with the MR-FOB without friction-shaping (i.e., $f_r = 0$) and the PD combined with the MR-FOB with friction-shaping considering $f_r = f_m$. Force responses are shown in Figure 7, where the change of environment impedance is highlighted by red dashed lines. Looking at the PD responses (plot (a)), one can observe how, without any friction compensation law, undesired friction significantly affects the control response, which is characterized by evident static errors that may manifest differently depending on the environment. These effects are reduced when employing the

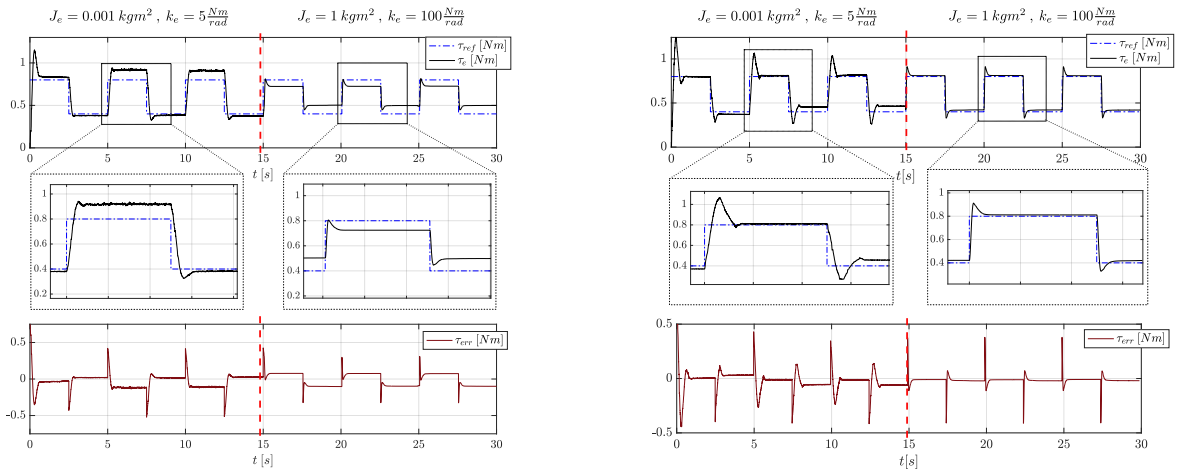

(a) PD

(b) PD + Model-Based

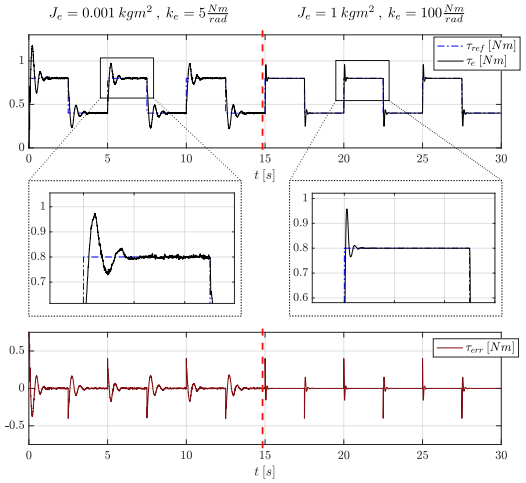

(c) PD + MR-FOB ($f_r = 0$)

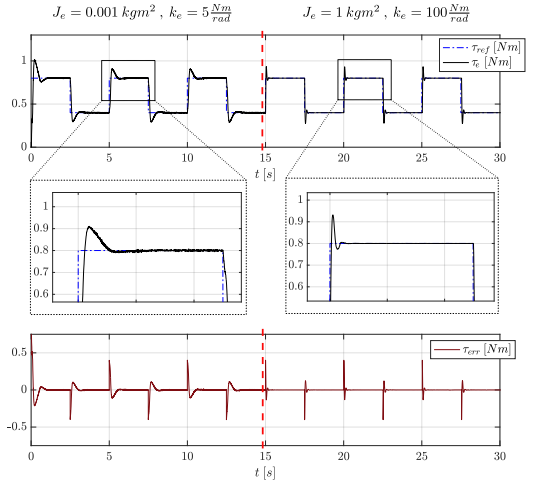

(d) PD + MR-FOB ($f_r = f_m$)

Fig. 7: Torque tracking considering an actuator interacting with a low-impedance and a high-impedance environment. Environment changes are highlighted by the red dashed line, whereas environment values are reported on top of the plots. Figure (a) considers a PD without any friction compensation law, Figure (b) considers the PD with a model-based friction compensation, Figure (c) considers the PD with the MR-FOB without friction-shaping (i.e., $f_r = 0$) and Figure (d) considers the PD with the MR-FOB with friction-shaping (i.e., $f_r = f_m$).

model-based friction compensator (plot (b)), which, however, still exhibits static errors. A quite significant improvement can be seen when employing the MR-FOB (plot (c)) which is tuned to fully compensate friction (i.e, $f_r = 0$). Even if static errors disappear, this solution leads to oscillatory behaviour when interacting with a soft environment. Finally, the MR-FOB set in friction-shaping mode (plot (d)) is the only solution showing null steady-state error and non-oscillatory responses in both environments. Indeed, friction-shaping helps to reduce overshoot and settling time with respect to responses in plot (c).

VI. CONCLUSIONS

This paper proposes a novel force control architecture that includes a model reference friction observer that allows for accurate compensation of friction effects without relying on a friction model. Since passivity is a fundamental requirement for interaction control, a passivity proof is provided, showing that the proposed solution preserves passivity at the control, environment, and friction ports by satisfying a simple condition on the observer parameters. This implies that the MR-FOB can perform a passive friction compensation for any friction profile and can be used in combination with any passive force controller while retaining a stable interaction with any passive environment. In addition, the proposed architecture exhibits beneficial friction-shaping capabilities

still being passive. The approach is validated through simulation and experimental trials, showing coherence with theoretical expectations.

REFERENCES

[1] X. Xue, H. Huang, L. Zuo, and N. Wang, "A compliant force control scheme for industrial robot interactive operation," *Frontiers in Neurorobotics*, vol. 16, 3 2022.

[2] R. V. Patel, S. F. Atashzar, and M. Tavakoli, "Haptic feedback and force-based teleoperation in surgical robotics," *Proceedings of the IEEE*, vol. 110, pp. 1012–1027, 7 2022.

[3] T. Proietti, V. Crocher, A. Roby-Brami, and N. Jarrasse, "Upper-limb robotic exoskeletons for neurorehabilitation: a review on control strategies," *IEEE Reviews in Biomedical Engineering*, vol. PP, no. 99, p. 1, 2016.

[4] S. Huang, W. Liang, and K. K. Tan, "Intelligent friction compensation: A review," *IEEE/ASME Transactions on Mechatronics*, vol. 24, pp. 1763–1774, 8 2020.

[5] V. Johansson, S. Moberg, E. Hedberg, M. Norrlöf, and S. Gunnarsson, "A learning approach for feed-forward friction compensation," in *IFAC-PapersOnLine*, vol. 51. Elsevier B.V., 1 2018, pp. 412–417.

[6] A. F. Guc, Z. Yumrukcal, and O. Ozcan, "Nonlinear identification and optimal feedforward friction compensation for a motion platform," *Mechatronics*, vol. 71, 11 2020.

[7] L. C. Bo and D. Pavelescu, "The Friction-Speed Relation and its Influence on the Critical Velocity of Stick-Slip Motion," *Wear*, vol. 82, pp. 277–289, 1982.

[8] P. Dahl, "A solid friction model," *Aerospace Corporation El Segundo, CA*, vol. 158, pp. Tech. Rep. TOR–01 58(3 107–1 8)– 1, 1968.

[9] C. Canudas de Wit, H. Olsson, K. Astrom, and P. Lischinsky, "A new model for control of systems with friction," *IEEE Transactions on Automatic Control*, vol. 40, no. 3, pp. 419–425, Mar. 1995.

[10] C. C. de Wit and P. Lischinsky, "Adaptive friction compensation with partially known dynamic friction model," *International Journal of Adaptive Control and Signal Processing*, vol. 11, no. 1, pp. 65–80, Feb. 1997.

[11] B. Bona, M. Indri, and N. Smaldone, "Rapid prototyping of a model-based control with friction compensation for a direct-drive robot," *IEEE/ASME Transactions on Mechatronics*, vol. 11, pp. 576–584, 10 2006.

[12] H. Yu, S. Huang, G. Chen, Y. Pan, and Z. Guo, "Human-Robot Interaction Control of Rehabilitation Robots with Series Elastic Actuators," *IEEE Transactions on Robotics*, vol. 31, no. 5, pp. 1089–1100, 2015.

[13] E. Sariyildiz and K. Ohnishi, "An adaptive reaction force observer design," *IEEE/ASME Transactions on Mechatronics*, vol. 20, no. 2, pp. 750–760, 2015.

[14] K. A. Verbert, R. Toth, and R. Babuska, "Adaptive Friction Compensation: A Globally Stable Approach," *IEEE/ASME Transactions on Mechatronics*, vol. 21, no. 1, pp. 351–363, 2016.

[15] T. H. Lee, K. K. Tan, and S. Huang, "Adaptive friction compensation with a dynamical friction model," *IEEE/ASME Transactions on Mechatronics*, vol. 16, no. 1, pp. 133–140, Feb. 2011.

[16] S. Huang, K. Tan, and T. Lee, "Adaptive friction compensation using neural network approximations," *IEEE Transactions on Systems, Man and Cybernetics, Part C (Applications and Reviews)*, vol. 30, no. 4, pp. 551–557, Nov. 2000.

[17] S. Huang and K. K. Tan, "Intelligent friction modeling and compensation using neural network approximations," *IEEE Transactions on Industrial Electronics*, vol. 59, pp. 3342–3349, 8 2012.

[18] G. Zhang and J. Furusho, "Control of robot arms using joint torque sensors," *International Conference on Robotics and Automation*, 1997.

[19] L. Le Tien, A. Albu-Schäffer, and A. De Luca, "Friction observer and compensation for control of robots with joint torque measurement," in *IEEE/RSJ International Conference on Intelligent Robots and System*, 2008, pp. 3789–3795.

[20] C. J. Lin, H. T. Yau, and Y. C. Tian, "Identification and compensation of nonlinear friction characteristics and precision control for a linear motor stage," *IEEE/ASME Transactions on Mechatronics*, vol. 18, no. 4, pp. 1385–1396, 2013.

[21] H. Qian and J. De Schutter, "Introducing Active Linear and Nonlinear Damping to Enable Stable High Gain Force Control in case of Stiff Contact," in *International Conference on Robotics and Automation*, 1992.

[22] C. Melchiorri, S. Stramigioli, and S. Andreotti, "Using damping injection and passivity in robotic manipulation," *IEEE/ASME International Conference on Advanced Intelligent Mechatronics, AIM*, pp. 979–984, 1999.

[23] W. T. Townsend and J. K. Salisbury, "The effect of coulomb friction and stiction on force control," in *IEEE International Conference on Robotics and Automation*, 1987, pp. 883–889.

[24] K. Kong, S. Member, and J. Bae, "Control of Rotary Series Elastic Actuator for Ideal Force-Mode Actuation in Human-Robot Interaction Applications," *IEEE/ASME Transaction on Mechatronics*, vol. 14, no. 1, pp. 105–118, 2009.

[25] N. Paine, J. S. Mehling, J. Holley, N. A. Radford, G. Johnson, C. L. Fok, and L. Sentis, "Actuator control for the NASA-JSC valkyrie humanoid robot: A decoupled dynamics approach for torque control of series elastic robots," *Journal of Field Robotics*, vol. 32, no. 3, pp. 378–396, 2015.

[26] E. Dimo and A. Calanca, "Environment Aware Friction Observer with Applications to Force Control Benchmarking," *Actuators*, vol. 13, no. 53, 2024.

[27] T. Murakami, F. Yu, and K. Ohnishi, "Torque Sensorless Control in Multidegree-of-Freedom Manipulator," *IEEE Transactions on Industrial Electronics*, vol. 40, no. 2, pp. 259–265, 1993.

[28] E. Sariyildiz and K. Ohnishi, "Stability and robustness of disturbance-observer-based motion control systems," *IEEE Transactions on Industrial Electronics*, vol. 62, pp. 414–422, 2015.

[29] G. A. Pratt and M. Williamson, "Series Elastic Actuators," in *International Conference on Intelligent Robots and Systems*, vol. 1. IEEE, 1995, pp. 399–406.

[30] A. Calanca, E. Dimo, R. Vicario, P. Fiorini, M. Serpelloni, and G. Legnani, "Introducing Series Elastic Links for Affordable Torque-Controlled Robots," *IEEE Robotics and Automation Letters*, vol. 4, no. 1, pp. 137–144, 2019.

[31] K. Ohnishi, M. Shibata, and T. Murakami, "Motion control for advanced mechatronics," *IEEE/ASME Transactions on Mechatronics*, vol. 1, no. 1, pp. 56–67, 1996.

[32] H. Kobayashi, S. Katsura, and K. Ohnishi, "An analysis of parameter variations of disturbance observer for motion control," *IEEE Transactions on Industrial Electronics*, vol. 54, pp. 3413–3421, 12 2007.

[33] E. Colgate and N. Hogan, "An Analysis Of Contact Instability In Terms Of Passive Physical Equivalents," in *IEEE International Conference on Robotics and Automation*, vol. 1, 1989, pp. 404 – 409.

[34] R. Vicario, A. Calanca, E. Dimo, N. Murr, M. Meneghetti, R. Ferro, E. Sartori, and T. Boaventura, "Benchmarking Force Control Algorithms," in *ACM International Conference Proceeding Series*, vol. 1, no. 1. Association for Computing Machinery, 2021, pp. 359–364.